catalysts

MDPI

Article

Kinetic Study on CO-Selective Methanation over Nickel-Based Catalysts for Deep Removal of CO from Hydrogen-Rich Reformate

Woohyun Kim, Khaja Mohaideen Kamal †, Dong Joo Seo * and Wang Lai Yoon *

Hydrogen Research Department, Hydrogen Energy Research Division, Korea Institute of Energy Research (KIER), 152 Gajeong-ro, Yuseong-gu, Daejeon 34129, Korea; wkim@kier.re.kr (W.K.); kkhaja@gmail.com (K.M.K.)

* Correspondence: djseo@kier.re.kr (D.J.S.); wlyoon@kier.re.kr (W.L.Y.)

† Present affiliation: Department of Catalysis and Chemical Reaction Engineering, National Institute of Chemistry, 1000 Ljubljana, Slovenia.

Abstract: The CO-selective methanation process is considered as a promising CO removal process for compact fuel processors producing hydrogen, since the process selectively converts the trace of CO in the hydrogen-rich gas into methane without additional reactants. Two different types of efficient nickel-based catalysts, showing high activity and selectivity to the CO methanation reaction, were developed in our previous works; therefore, the kinetic models of the reactions over these nickel-based catalysts have been investigated adopting the mechanistic kinetic models based on the Langmuir chemisorption theory. In the methanation process, the product species can react with the reactant and also affect the adsorption/desorption of the molecules at the active sites. Thus, the kinetic parameter study should be carried out by global optimization handling all the rate equations for the plausible reactions at once. To estimate the kinetic parameters, an effective optimization algorithm combining both heuristic and deterministic methods is used due to the large solution space and the nonlinearity of the objective function. As a result, 14 kinetic parameters for each catalyst have been determined and the parameter sets for the catalysts have been compared to understand the catalytic characteristics.

Keywords: CO-selective methanation; nickel catalysts; kinetic parameters; genetic algorithm; parameter estimation

Citation: Kim, W.; Kamal, K.M.; Seo, D.J.; Yoon, W.L. Kinetic Study on CO-Selective Methanation over Nickel-Based Catalysts for Deep Removal of CO from Hydrogen-Rich Reformate. *Catalysts* **2021**, *11*, 1429. https://doi.org/10.3390/catal11121429

Academic Editors: Anastasia Macario and Jaroslaw Polanski

Received: 11 October 2021
Accepted: 20 November 2021
Published: 24 November 2021

1. Introduction

There has been growing interest in generating electric energy from hydrogen due to serious concerns about climate change brought about by greenhouse gases. The combination of a methane-steam reformer and polymer electrolyte membrane fuel cells (PEMFCs) has been considered as an effective distributed power source due to the development of compact and low-cost fuel processors and the scalability of the fuel cell system [1–4]. In this combined system, hydrogen-rich gas fed into the PEMFCs is produced via steam reforming and water–gas shift (WGS) reactions [3,4]. The fraction of CO in the reformate gas after the WGS process is approximately 0.5–1 vol.% and it should be reduced preferably to less than 10 ppm for the platinum catalyst in the anode of low-temperature PEMFCs; otherwise, a drastic deactivation of the fuel cell anodes by CO poisoning arises. Preferential CO oxidation (PROX: $CO + 0.5\ O_2 \rightarrow CO_2$) has been widely used for deep CO removal in a compact fuel processor combined with low-temperature PEMFCs [2–4]. Although PROX has been practiced in commercial compact fuel processors, this process requires air (oxygen) supply and cooling systems to avoid undesired loss of hydrogen, which make the fuel processors complex and costly [5,6]. On the other hand, as depicted in Figure 1, the CO-selective methanation (CO-SELMET: $CO + 3H_2 \rightarrow CH_4 + H_2O$) process is considered as an effective alternative because the direct hydrogenation of CO occurs over proper catalysts without an additional reactant supply. Thus, the CO-SELMET process can be a practical

and cost-effective solution to the development of the compact fuel processor combined with low-temperature PEMFCs [5–8].

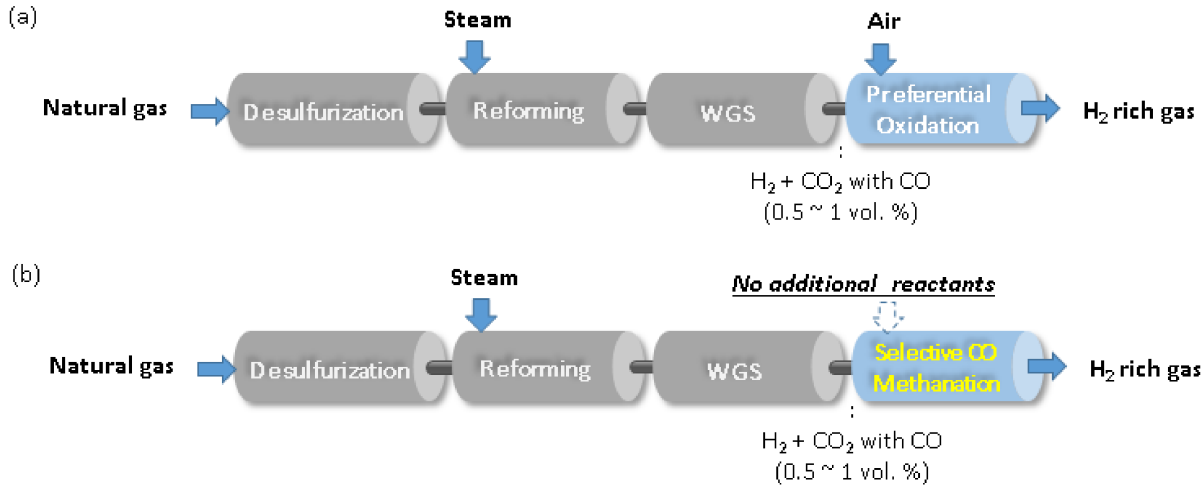

Figure 1. Comparison between two different CO-removal processes for a fuel processor: (**a**) PROX and (**b**) CO-SELMET processes.

According to the published reports on CO-SELMET catalysis over the last few decades, nickel- and ruthenium-based catalysts have been attracting a great deal of attention [5–23]. Specifically, among the various experimental results, Ru-based catalysts (e.g., Ru/TiO_2) have shown consistently high activity and selectivity to CO [15–19]. Despite the remarkable performance of the Ru-based catalyst, Ni is considered commercially appropriate as a major component due to economic aspects. Consequently, highly efficient nickel-based catalysts, showing outstanding performance under the condition similar to the actual reformate gas, can be a more practical solution to the commercialization of the CO-SELMET process [5,6,13,21–23].

Although a great deal of previous research studies on catalytic preparations and morphological analyses have been reported, kinetic studies on CO-SELMET catalysis have barely been carried out. In fact, a mechanistic kinetic model for the CO methanation reaction over ordinary nickel catalysts has intensively been investigated since the 1970s [24–28]. Then, recently, kinetic studies on the CO_2 methanation process, utilizing captured CO_2 or CO_2-rich biogas, were also reported [29–32]. However, most of the previous research studies deal with independent CO and CO_2 methanation reactions under the condition where no steam exists in the feed gas. They are not applicable for developing global kinetic models of all the plausible reactions in the CO-SELMET process for deep CO removal from hydrogen-rich reformate gas because there must be competitive CO and CO_2 reactions, e.g., methanation and WGS reactions, due to the existence of CO, CO_2 and residual steam. Thus, the objective of this work is to develop global kinetic models regarding all plausible reactions in the CO-SELMET process. For an exemplary practice, we have investigated the kinetics of the reactions in the CO-SELMET process over the two different types of nickel-based catalysts suggested in our previous research studies for comparison: (1) the iridium-doped nickel catalyst [5] and (2) the nickel-zirconium composite catalyst [21]. In order to determine appropriate mechanistic kinetic models for the catalytic reactions, the Langmuir–Hinshelwood models have been adopted according to the previous research studies on reaction mechanisms and all the parameters of the kinetic models have been globally determined by the efficient optimization algorithm, combining both heuristic and deterministic methods.

2. Results and Discussion

2.1. Mechanistic Reaction Model and Kinetic Parameter Estimation Method

The CO-SELMET process for deep CO removal from the hydrogen-rich gas produced by fuel processors deals with three competitive reactions: WGS or reverse WGS (RWGS), CO and CO_2 methanation reactions, as follows:

CO methanation reaction: $CO + 3H_2 \rightarrow CH_4 + H_2O$ $\Delta H^o = -206$ kJ/mol (at 298 K)

CO_2 methanation reaction: $CO_2 + 4H_2 \rightarrow CH_4 + 2H_2O$ $\Delta H^o = -165$ kJ/mol (at 298 K)

WGS/RWGS reactions: $CO + H_2O \leftrightarrow CO_2 + H_2$ $\Delta H^o = -41$ kJ/mol (at 298 K)

It is generally accepted that CO methanation proceeds via adsorption of CO and H_2 on the active metal sites and dissociation followed by the hydrogenation of the adsorbed carbonaceous species [25–28]. However, the CO_2 methanation mechanism is explained in a different way: CO_2 is firstly adsorbed on the catalyst support surface, and then, the hydrogenation reaction follows possibly at the active metal–support interface so CO_2 adsorption does not compete with CO according to this explanation [33,34]. In addition to the two methanation reactions, WGS and RWGS reactions also occur in the CO-SELMET process due to the coexistence of CO, CO_2 and steam. Based on the chemisorption mechanisms and the reaction equilibrium theory, well-accepted mechanistic kinetic studies were already proposed in the 1980s [35,36].

To develop the kinetic models of all these possible reactions in the CO-SELMET process, we have adopted the Langmuir chemisorption theory so the rate Equations (1)–(3) are derived as reported in a number of published works since the 1980s [24–31,35,36]. Using the kinetic models and stoichiometry, the generation or consumption rate of each species can be expressed as the ordinary differential forms (Equations (4)–(9)). The balance Equations (4)–(9) are valid under the assumption that the only three reactions occur in the catalytic reaction system. This assumption is confirmed by calculating the carbon balance in the reaction experiments, which will be briefly discussed in the next section. In addition, it should be noted that the optimal kinetic parameters have to be globally determined because all the plausible reactions simultaneously occur. In other words, the reactions cannot separately occur: for example, if CO and H_2 are fed into the reactor for the methanation reaction, CO can also react with the steam (WGS) formed via the methanation reaction.

Then, the dry-basis compositions of the product gas can be calculated by Equation (10) and be compared with the experimentally measured data. Thus, the kinetic parameters should be optimally determined to minimize the differences between the predicted and the measured values. Thus, as mentioned above, the kinetic parameters are globally determined unlike a number of previous works focusing on the separate kinetic model.

CO methanation rate [mol/h/g_{cat}]:

$$r_{CO,m} = -\frac{k_m K_{CO} K_{H_2}^2 P_{CO} P_{H_2}^2}{\left(1 + K_{CO} P_{CO} + K_{H_2} P_{H_2}\right)^2} \quad (1)$$

WGS reaction rate [mol/h/g_{cat}]:

$$r_{CO,wgs} = -\frac{k_{wgs}/P_{H_2}\left(P_{CO}P_{H_2O} - P_{H_2}P_{CO_2}/K_{eq,wgs}\right)}{\left(1 + K_{CO}P_{CO} + K_{H_2}P_{H_2} + K_{H_2O}P_{H_2O}/P_{H_2}\right)^2} \quad (2)$$

CO_2 methanation rate [mol/h/g_{cat}]:

$$r_{CO_2,m} = -\frac{k_{m2}\left(P_{CO_2}P_{H_2}\right)^{0.5}}{\left(1 + \left(K_{H_2}P_{H_2}\right)^{0.5} + \left(K_{CO_2}K_{H_2}P_{CO_2}P_{H_2}\right)^{0.5} + \frac{K_{H_2O}P_{H_2O}}{P_{H_2}}\right)^2} \quad (3)$$

where

P_i: partial pressure of species i (i = CO, CO_2, CH_4, H_2 and H_2O) [bar];

$K_{eq,wgs} = e^{\frac{4577.8}{T} - 4.33}$: equilibrium constant of WGS [37], $k_i = A_i e^{-\frac{Ea_i}{RT}}$ and $K_j = B_j e^{-\frac{\Delta H_j}{RT}}$

Balance equations for the species:

$$\frac{dF_{H_2O}}{dw} = r_{H_2O} = -r_{CO,m} + r_{CO,wgs} - 2 \times r_{CO_2,m} \quad (4)$$

$$\frac{dF_{CO}}{dw} = r_{CO} = r_{CO,m} + r_{CO,wgs} \quad (5)$$

$$\frac{dF_{H_2}}{dw} = r_{H_2} = 3 \times r_{CO,m} - r_{CO,wgs} + 4 \times r_{CO_2,m} \quad (6)$$

$$\frac{dF_{CO_2}}{dw} = r_{CO_2} = -r_{CO,wgs} + r_{CO_2,m} \quad (7)$$

$$\frac{dF_{N_2}}{dw} = 0 \quad (8)$$

$$\frac{dF_{CH_4}}{dw} = r_{CH_4} = -r_{CO,m} - r_{CO_2,m} \quad (9)$$

Dry-basis composition at the outlet of the catalyst bed, calculated in the model [%]:

$$C_{i,out} = \frac{F_{i,out}}{(F_{CO,out} + F_{H_2,out} + F_{CO_2,out} + F_{N_2,out} + F_{CH_4,out})} \times 100 \quad (10)$$

where

$$W = \int_{F_{i,in}}^{F_{i,out}} \frac{dF_i}{r_i}$$

$F_{i,in}$ and $F_{i,out}$: molar flow rate of species i at the inlet and outlet of the catalyst bed (i = CO, CO_2, CH_4, H_2 and H_2O) [mol/h];
r_i: generate or consumption rate of species i (i = CO, CO_2, CH_4, H_2 and H_2O) [mol/h/g_{cat}]
W: weight of the catalyst bed [g].

For the kinetic experiments, a fixed-bed quartz reactor was used, and the pressure was maintained at the atmospheric level. Multiple experiments where the temperature and gas compositions were varied in the wide ranges (see Table 1) were carried out and the measured dry-basis molar composition of each species was used for the kinetic parameter estimation. Cases 1 and 2, CO and CO_2 methanation reactions, are separated and Case 3 is similar to the gas compositions of the actual reformate gas from an ordinary natural-gas-based fuel processor. Detailed information on the experiments, such as catalyst preparation, experimental apparatus, etc., is provided in Section 3.

Table 1. Experimental conditions for kinetic parameter estimation.

Experiment	GHSV (/h)	Temperature (°C)	Gas Composition (vol.%)
Case 1	8400/h	150–250	1% CO, 0% CO_2, 78.9% H_2, 15.2% steam and 4.9% N_2
Case 2			0% CO, 20% CO_2, 59.9% H_2, 15.2% steam and 4.9% N_2
Case 3			1% CO, 20% CO_2, 58.9% H_2, 15.2% steam and 4.9% N_2

To define the kinetic parameters, an optimization problem is defined. The objective function for the kinetic parameter estimation is shown as Equation (11), which is an ordinary root means square error equation, and this complicated optimization problem has been solved using the genetic algorithm (GA), which is a widely used heuristic optimization method for parameter estimation because of the non-linearity and the extremely large solution space of the objective function [38,39]. However, the heuristic optimization methods cannot guarantee the optimality of the solutions and may require a number of ineffective iterations near the optimal solutions. Therefore, combination with a deterministic optimization method can provide synergic effects, reducing the aforementioned drawbacks of the GA when solving such high-dimensional optimization problems [38–41]. Thus, we have used the GA combined with the fmincon function in the Global Optimization Toolbox 8.0 of MATLAB R2017b [39] and the ordinary differential equations (ODE) were solved using the ode23t solver, which is the common MATLAB ODE solver for stiff functions. Thus, the 14 kinetic parameters for each catalyst were estimated with the experimental data. For the parameter estimation trials, approximately 400–1000 iterations were carried out by the GA to find the best solution. The detailed options for the kinetic parameter estimation are summarized in Table 2.

Table 2. Relevant options of the GA combined with the deterministic algorithm for kinetic parameter estimation.

Number of Populations	Fitness Scaling	Selection	Reproduction	Mutation	Crossover	Hybrid Function
200	Rank	Stochastic uniform	Elite count: 4 Crossover fraction: 0.8	Adaptive feasible	Constraint dependent	fmincon

Objective function:

$$\min f(KP) = \sqrt{\frac{\sum_{i=1}^{n}\left[\left(C_{i,out} - C_{i,out}^{exp}\right)^2\right]}{n}} \quad (11)$$

Subject to LB < KP < UB
where

$$KP = \left[A_m,\ A_{wgs},\ A_{m2},\ B_{CO},\ B_{H_2},\ B_{CO_2},\ B_{H_2O}, Ea_m,\ Ea_{wgs},\ Ea_{m2},\ \Delta H_{CO},\ \Delta H_{H_2}\ \Delta H_{CO_2}\ \Delta H_{H_2O}\ \right]$$

$$LB = [0, 0, 0, 0, 0, 0, 0, 0, 0, 0, -100, -100, -100, -100]$$

$$UB = \left[10^{18}, 10^{18}, 10^{18}, 10, 10, 10, 10^5, 3\times10^5, 3\times10^5, 3\times10^5, 10^5, 10^5, 10^5, 10^5,\right]$$

n = the number of experimental data;
KP: set of kinetic parameters to be estimated;
LB: lower bound constraint;
UB: upper bound constraint.

2.2. Parameter Estimation Results

2.2.1. Ir/Ni-MgO/γ-Alumina and $Ni_{0.5}Zr_{0.5}O_2$ Catalyst

The experimental data and the kinetic model predictions for both Ir/Ni-MgO/γ-alumina and $Ni_{0.5}Zr_{0.5}O_2$ catalysts are illustrated in Figures 2 and 3, comparing the compositions of the carbonaceous species. It should be noted that the absence of side reactions other than the three main reactions mentioned above was confirmed by the carbon balance calculations made at all data points of these experiments.

To discuss the reaction phenomena and kinetic properties of the Ir/Ni-MgO/γ-alumina catalyst, in Case 1, the CO_2 methanation is considered negligible and the tiny amount of CO is consumed by both the hydrogenation and the WGS reactions. The experimental data show that the CO methanation reaction is readily accelerated from 190 °C (see Figure 2a). On the other hand, CO_2 is considered to be generated by only the WGS ($CO + H_2O \rightarrow CO_2 + H_2$) reaction in Case 1. Figure 2a shows that the CO_2 concentration starts to increase at or above 190 °C, but remains under 0.04 mol%. In Case 2, CO_2 methanation is expected to be dominant in the hydrogen-rich gas without CO feeding. For the sake of an efficient deep CO removal process where the residual CO centration has to be maintained below a few dozen ppm, the catalyst should be designed to suppress the CO_2 reaction, avoiding unnecessary consumption of hydrogen in the reformate gas. When using the Ir/Ni-MgO/γ-alumina catalyst, the increase in CH_4 concentration by the hydrogenation of CO_2 in the product gas is observed from 230 °C, despite the abundant amount of CO_2 and hydrogen, as shown in Figure 2b. This means that the CO_2 hydrogenation is efficiently suppressed under 230 °C. This is the most important attribute of the CO-SELMET catalyst for the deep removal of CO in the reformate gas [5–10,21,33,34]. Finally, in Case 3, the reactions proceed under conditions similar to the actual CO-SELMET process applied to the ordinary fuel processor having a methane-steam reformer followed by a WGS reactor. The catalyst selectively and efficiently converts the CO into CH_4, minimizing the undesired hydrogen loss by CO_2 methanation up to 230 °C (see Figure 2c).

Such high activity and selectivity to CO molecules are also confirmed by the estimated kinetic parameters. A comparison between k_m and k_{m2} values (reaction frequency factors at the active site of the catalyst for CO and CO_2 hydrogenation reactions, respectively) is shown in Figure 4a,b. They help understand the aforementioned mutually competitive hydrogenation reactions: the k_m value of the Ir/Ni-MgO/γ-alumina catalyst has a far larger order of magnitude than its k_{m2} value in the whole temperature range, which means the CO hydrogenation rate is approximately 10^9 times faster than

the CO_2 hydrogenation rate. In order to understand such a remarkable difference in the k_m and k_{m2} values, the estimated kinetic parameters should be discussed as follows: in Table 3, it is found that the activation energy of the CO methanation reaction (Ea_m = 185.647 kJ/mol) of the Ir/Ni-MgO/γ-alumina catalyst is much lower than the one of CO_2 methanation (Ea_{m2} = 272.479 kJ/mol). However, its adsorption parameters related to CO and CO_2 reveal the relatively stronger preference for CO_2 over CO (see Table 4), which may not be helpful to maintain the high selectivity of the catalyst to CO molecules. In other words, although the adsorption of CO_2 molecules is favorable, the reaction rate of CO hydrogenation at the active sites of the Ir/Ni-MgO/γ-alumina catalyst is excessively faster than the CO_2 hydrogenation. This is the way that the Ir/Ni-MgO/γ-alumina catalyst efficiently and selectively removes CO, avoiding the CO_2 reaction.

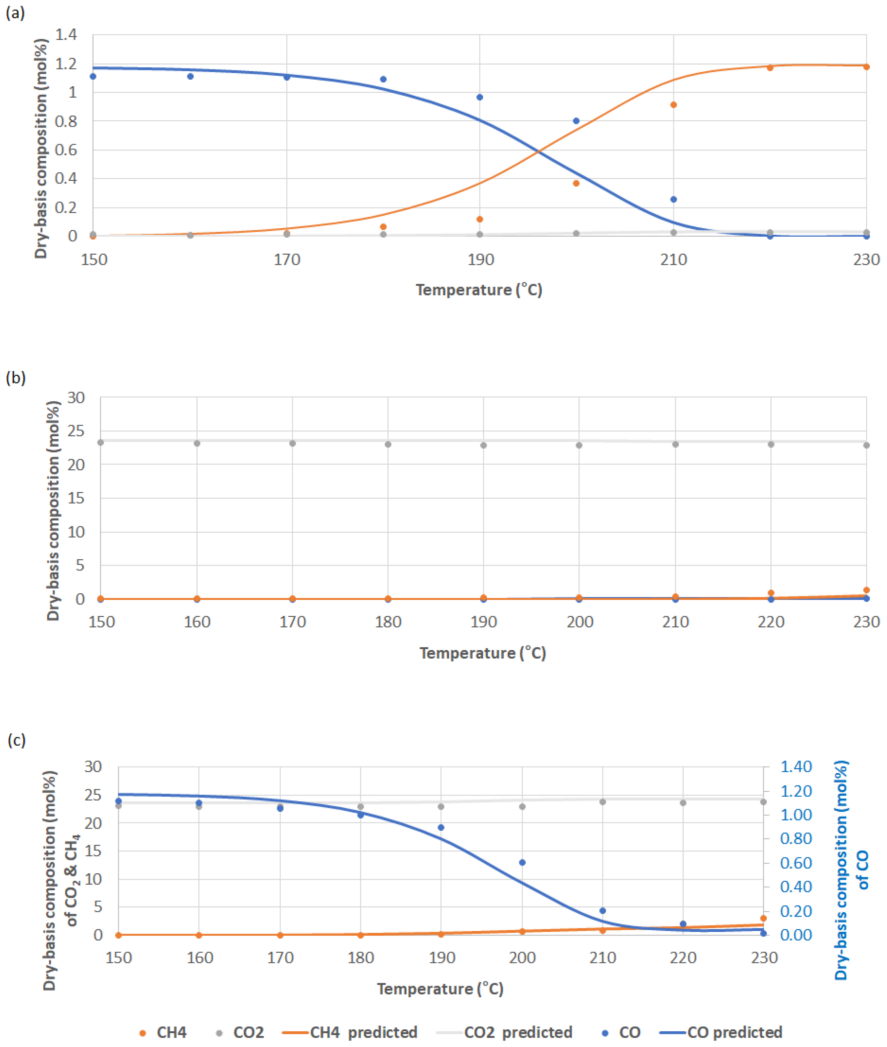

Figure 2. Comparison between the prediction of the developed kinetic models and the experimental data when using the Ir/Ni-MgO/γ-alumina catalyst ((**a**): Case 1, (**b**): Case 2, (**c**): Case 3).

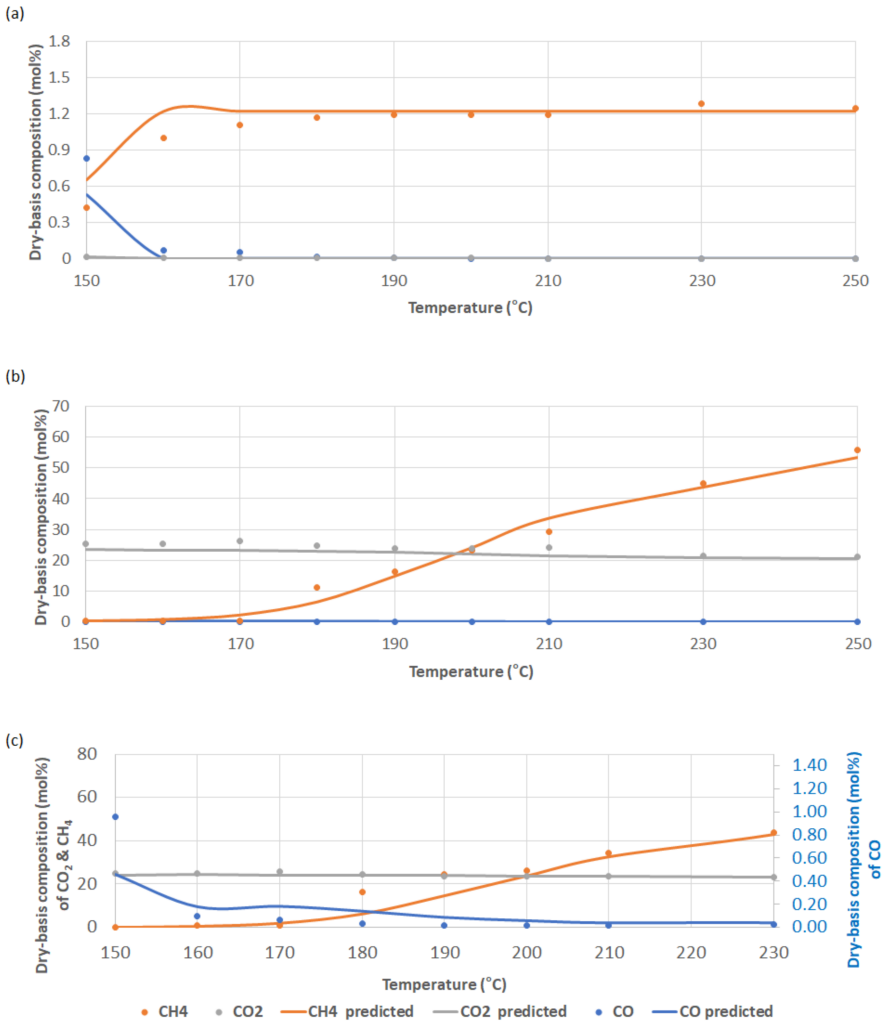

Figure 3. Comparison between the prediction of the developed kinetic models and the experimental data when using the $Ni_{0.5}Zr_{0.5}O_2$ catalyst ((**a**): Case 1, (**b**): Case 2, (**c**): Case 3).

Table 3. Pre-exponential factors and activation energies for both catalysts.

Catalyst	Parameters of the Arrhenius Equation					
	A_m $(\times 10^{15})$	A_{wgs} $(\times 10^{15})$	A_{m2} $(\times 10^{15})$	Ea_m (kJ/mol)	Ea_{wgs} (kJ/mol)	Ea_{m2} (kJ/mol)
Ir/Ni-MgO/γ-alumina	881.042	452.152	632.149	185.647	16.967	272.479
$Ni_{0.5}Zr_{0.5}O_2$	522.722	3.213	46.657	189.647	19.083	67.834
Ni/γ-alumina [24]	2.09×10^{-10}		1.36×10^{-3}	226.2		106.3
Ni catalyst [28]				105.9		
Ni/alumina [30]	4.8×10^{-6}	7.83×10^{-9}		103	21	

Table 4. Adsorption parameters for both catalysts.

Catalyst	Adsorption Parameters							
	B_{CO}	B_{H2}	B_{CO2}	B_{H2O} $(\times 10^3)$	ΔH_{CO} (kJ/mol)	ΔH_{H2} (kJ/mol)	ΔH_{CO2} (kJ/mol)	ΔH_{H2O} (kJ/mol)
Ir/Ni-MgO/γ-alumina	8.515	2.227	6.412	3.792	−12.057	−74.309	−65.430	1.000
$Ni_{0.5}Zr_{0.5}O_2$	2.702	0.002	0.010	99.789	−65.841	−53.603	−79.935	1.306
Ni/γ-alumina [24]	4.56×10^{-4}				−52.1			
Ni catalyst [28]								
Ni/alumina [30]	8.23×10^{-5}	6.12×10^{-9}		177	−70.7 *	82.9 *		88.7 *

*: Reproduced from [35], AIChE J.: 1989.

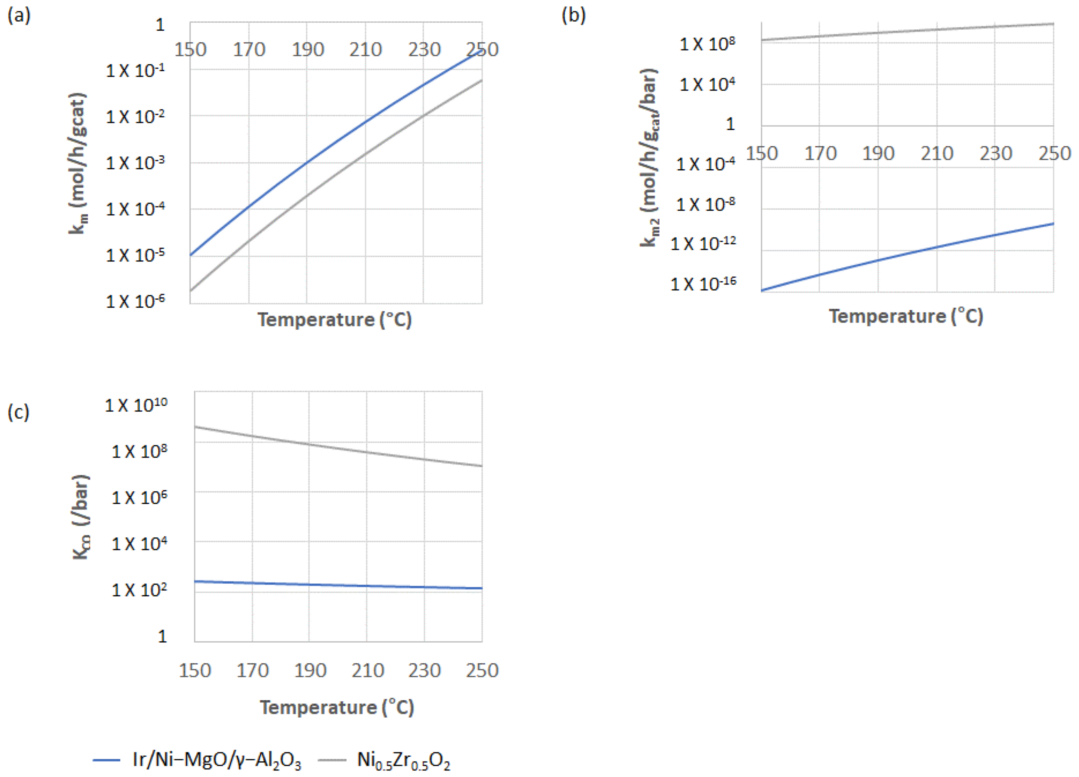

Figure 4. The calculated k_m, k_{m2} and K_{CO} values ((**a**–**c**), respectively) of the Ir/Ni-MgO/γ-alumina (blue line) and the $Ni_{0.5}Zr_{0.5}O_2$ catalysts (grey line).

Following the same manner for the Ir/Ni-MgO/γ-alumina catalyst, the kinetic parameters for the $Ni_{0.5}Zr_{0.5}O_2$ catalyst are also determined, and the model prediction results and the experimental data are compared and shown in Figure 3. First of all, in Case 1, the $Ni_{0.5}Zr_{0.5}O_2$ catalyst readily removes CO by accelerating the hydrogenation reaction from 150 °C, faster than the Ir/Ni-MgO/γ-alumina catalyst, and the CO_2 concentration is nearly zero in the whole range of the temperature. This means that the RWGS reaction may not have occurred yet, or even if the RWGS reaction generates a small amount of CO_2, it is rapidly converted into CH_4 by the hydrogenation reaction. The experimental data of Case 2 show the stronger activity to CO_2 compared with the Ir/Ni-MgO/γ-alumina catalyst (compare the CH_4 compositions in Figures 2b and 3b). The undesired hydrogen consumption by the CO_2 hydrogenation is the drawback of the catalyst. In spite of the strong activity to the CO_2 hydrogenation reaction, the catalyst removes CO under the condition similar to the actual reformate gas (Case 3), as shown in Figure 3c. As the temperature increases, the RWGS reaction ($CO_2 + H_2 \rightarrow CO + H_2O$) can produce CO and the CO molecules are probably converted into methane, resulting in a high concentration of methane in the product gas.

The aforementioned differences in kinetic parameters are also considered for the $Ni_{0.5}Zr_{0.5}O_2$ catalyst. The k_m values of the $Ni_{0.5}Zr_{0.5}O_2$ catalyst are less than the ones of the Ir/Ni-MgO/γ-alumina catalyst (see Figure 4a), which means that the CO hydrogenation rate at the active sites of the Ir/Ni-MgO/γ-alumina catalyst is faster. On the other hand, the k_{m2} values of the $Ni_{0.5}Zr_{0.5}O_2$ catalyst are approximately 10^{30} times higher than the ones of the Ir/Ni-MgO/γ-alumina catalyst, as shown in Figure 4b, which demonstrates the extremely stronger activity to CO_2 and the simultaneous decrease in the CO selectivity. The lower activation energy for the CO_2 hydrogenation reaction (E_{am2}), shown in Table 3, corresponds to a strong activity to CO_2.

In addition to the comparison of the surface reaction rates (k_m and k_{m2}), adsorption characteristics also contribute to the overall reaction rate. The strong activity of the $Ni_{0.5}Zr_{0.5}O_2$ catalyst to CO can be explained by its adsorption characteristics. The stronger adsorption energy of CO (ΔH_{CO} = −66.144 kJ/mol for the $Ni_{0.5}Zr_{0.5}O_2$ catalyst and −12.057 kJ/mol for the Ir/Ni-MgO/γ-alumina catalyst in Table 3) is able to increase the surface concentration of the activated CO molecules, resulting in high K_{CO} values. The K_{CO} can contribute to the acceleration of the CO hydrogenation reaction (see the reaction rate equation of $r_{CO,m}$). This is the key difference between the two catalysts in controlling the CO-removal reaction rate: the Ir/Ni-MgO/γ-alumina catalyst has the fast and selective surface reaction and the $Ni_{0.5}Zr_{0.5}O_2$ catalyst has a stronger affinity to the CO molecules.

Lastly, for the WGS reaction, both the developed nickel-based catalysts have similar kinetic parameters. The WGS reaction under this circumstance is more dependent on the reaction equilibrium defined by temperature and pressure [35,36]. In the high temperature (>250 °C) condition, due to the RWGS reaction, deep CO removal, maintaining a ppm-level CO concentration, becomes difficult [5–10,21,33,34].

In terms of the accuracy of the kinetic model for the catalyst, the predicted values based on the optimally estimated parameters show good agreement with the experimental data, as shown in Figures 2 and 3 and Figure S1. Thus, the estimated kinetic parameters are considered to provide acceptable analyses for the reaction characteristics. As discussed so far, the estimated kinetic parameters will be compared with other published works dealing with various nickel-based methanation catalysts in the next section, so the validity and physicochemical properties of the estimated kinetic parameters can be discussed.

2.2.2. Comparisons of the Kinetic Parameters with Other Ni-Based Catalysts

The kinetic parameters of the two developed nickel-based catalysts showing the outstanding CO-removal performance are compared with published works dealing with nickel-based CO and/or CO_2 methanation catalysts [24,28,30]. Though the catalysts differ in nickel content, support and preparation method, they use the same active metal. Thus, some kinetic parameters can be compared with the results of this study, despite the fact that somewhat different kinetic models and related assumptions are employed.

Firstly, in terms of the CO methanation reaction, pre-exponential factors cannot be directly compared because the published papers adopt different kinetic models in detail, e.g., definition of the denominator in the kinetic models based on the Langmuir chemisorption theory, the power of the partial pressure of CO, etc. Instead, the activation energies, which is one of the most important catalytic properties related to the temperature dependence, can be essentially compared. As shown in Table 3, in the published works, the activation energy values of the CO methanation reaction (Ea_m) are in the range of 100–230 kJ/mol. The Ea_m values of the Ir/Ni-MgO/γ-alumina and the $Ni_{0.5}Zr_{0.5}O_2$ catalysts are approximately 190 kJ/mol, so the estimated parameters are considered feasible. Secondly, in this way, the activation energies (Ea_{m2}) of the CO_2 hydrogenation reaction can also be compared: they increase in the order of $Ni_{0.5}Zr_{0.5}O_2$ < Ni/γ-alumina < Ir/Ni-MgO/γ-alumina. The relatively strong activity of the $Ni_{0.5}Zr_{0.5}O_2$ catalyst to CO_2 is confirmed in the experiments as discussed in the previous section; the Ir/Ni-MgO/γ-alumina catalyst, on the other hand, efficiently suppresses the CO_2 reaction, resulting in higher selectivity to CO. Although all catalysts use nickel as an active species, it has been confirmed that the activation energy values (Ea_m and Ea_{m2}) are varying in the wide range. Such difference probably depends on the content of nickel, dispersion degree, support, etc., and as a result, these have direct effects on the activity and selectivity to both CO and CO_2 molecules. Lastly, the kinetic parameters for the WGS reaction have also been compared. It is obvious that all the Ea_{WGS} values of the different Ni-based catalysts remain similar in Table 3.

Regarding adsorption characteristics, only the adsorption energies of the CO molecule with respect to the different nickel-based catalysts can be compared due to the lack of information on other adsorption/desorption parameters. All the ΔH_{CO} values are in a similar order of magnitude so the parameters determined in this study seem to be in an

acceptable range. Comparing ΔH_{H2} and ΔH_{H2O} with Xu and Forment's work [35], the difference between the two catalysts is relatively notable. Xu and Froment specifically estimated the kinetic parameters in the steam-methane reforming process where the reaction temperature is much higher (generally around 700–800 °C) and the partial pressures of species (CH_4, CO, CO_2 and steam) are far different from the selective CO methanation process. In addition, Xu and Froment used the nickel supported on Mg spinel catalyst. Except the active metal, the support, promoter and preparation methods are different from the two catalysts that we developed. These aspects may affect the competitive adsorption characteristics, resulting in different adsorption parameters.

3. Materials and Methods

In this work, the two aforementioned outstanding catalysts, Ir/Ni-MgO/γ-alumina and $Ni_{0.5}Zr_{0.5}O_2$ catalysts, were prepared according to the published works [5,21]. To prepare the Ir/Ni-MgO/γ-alumina catalyst, first of all, Ni-MgO/γ-Al_2O_3 catalysts were prepared by the deposition–precipitation method using $Ni(NO_3)_2(H_2O)_6$ (Aldrich), $Mg(NO_3)_2(H_2O)_6$ (Aldrich) and γ-Al_2O_3 (PURALOX SCFa-140, SASOL) supports. The precipitation pH of the solution was adjusted at 11 with 10 wt.% KOH solution as a precipitation agent. The contents of the nickel and the magnesium were 30 wt.% and 5 wt.% in their metallic state, respectively. The solution was stirred at 80 °C for 24 h and then, it was filtered and washed several times with deionized water. The filtered powder was dried at 80 °C overnight and then, it was calcined at 400 °C for 1 h, where the rate of the temperature increase was 1 °C/min. After that, $IrCl_3 \cdot xH_2O$ (Aldrich) was used as Ir precursor so 1 wt.% was impregnated onto the nickel catalyst by the incipient wetness method. Then, it was calcined again in the same manner mentioned above [5]. The $Ni_{0.5}Zr_{0.5}O_2$ catalysts was prepared using $ZrO(NO_3)_2$ (Aldrich) as zirconium precursor and $Ni(NO_3)_3 \cdot 9H_2O$ (Junsei) as Ni precursor, where the molar ratio of Ni and Zr is 1:1. They were taken and dissolved separately in a minimum amount of distilled water. Urea (1 mol per metal ion) was also dissolved separately in a minimum amount of distilled water. Then, all these three solutions were mixed thoroughly by ultrasonicating for 2 min. The mixed solution was then transferred to a crystallizing dish, and it was heated on a laboratory hot plate at 200 °C. The resulting solid products were further heated at 400 °C for 1 h to obtain the nanostructured $Zr_{0.5}Ni_{0.5}O_2$ catalyst powders [21].

For the experiments, a fixed-bed quartz reactor (outer diameter: 0.5 inch) was used and the pressure was maintained at the atmospheric level. The prepared catalyst powder was pressed into a tablet and then crushed and sieved. The size of the sieved particles was less than 75 μm and the volume of the catalyst bed was 0.8 mL. For accurate analysis of the intrinsic activity, the particle size was studied with the pre-experiments so it is confirmed that approximately 75 μm powder catalysts had no (or minimized) diffusion resistance. The reaction temperature was monitored by a thermocouple placed at the center of the catalyst bed and the bed temperature is thoroughly controlled by the temperature-programmed PID controller (KP-1000, Chino, Tokyo, Japan). Before the reaction, the catalyst was reduced under the optimized reduction conditions [5,21]. The product gas passed through a water trap to condensate and remove the residual steam, and then, the gas compositions were analyzed with an on-line gas chromatograph (Agilent 6890 GC, Agilent Technologies, Inc., Santa Clara, CA, USA) equipped with both a thermal conductivity detector (TCD, for N_2) and a flame ionization detector (FID, for CO, CO_2 and CH_4) with a catalytic methanizer. To make the data consistent, the reaction temperature was held at each point for one hour so that the gas compositions measured by the GC remained stable. The concept of the experimental apparatus used in this work is depicted in Figure 5.

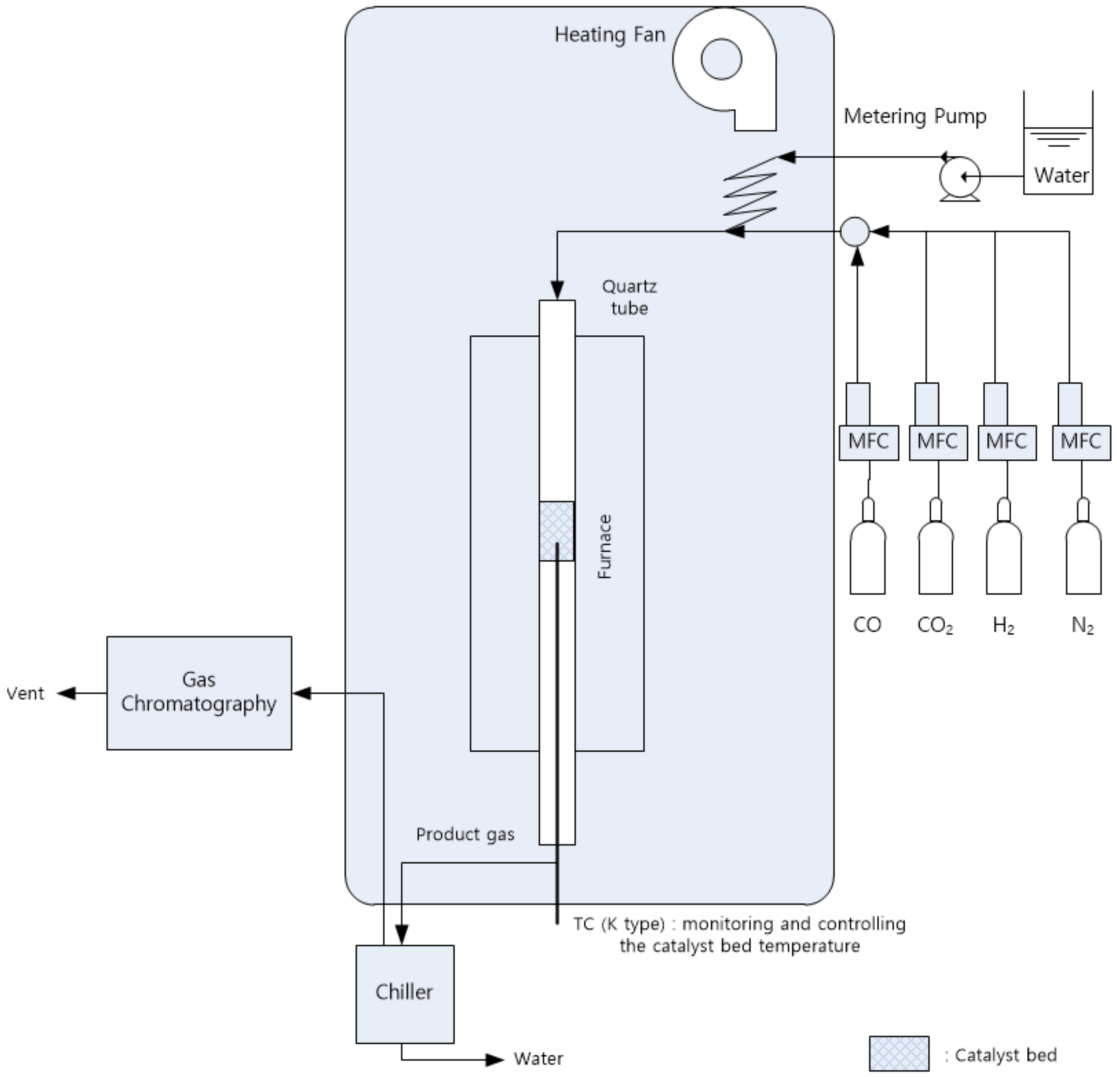

Figure 5. Configuration of the experimental apparatus.

4. Conclusions

The kinetic models of the two different nickel-based catalysts for the CO-SELMET process have been developed based on the Langmuir chemisorption theory using an efficient optimization method combining the GA and the deterministic algorithm. The globally determined parameters showed acceptable predictions of the overall reaction rates in wide ranges of reaction temperature. In addition, comprehensive explanations on the different catalytic characteristics for the catalysts have been provided, considering the kinetic parameters related to each plausible reaction. Thus, the differences in mechanistic kinetics, such as the activity and selectivity to CO and CO_2 molecules, for the reactions in a mutually competing relationship, are clearly explained. Accordingly, the methodology of this kinetic study can be useful to (1) understand catalytic properties, (2) optimize or modify the efficient catalysts (3) determine optimal operating windows with respect to the catalysts and (4) optimize the deep CO removal reactor comprising efficient CO-SELMET catalysts.

Supplementary Materials: The following are available online at https://www.mdpi.com/article/10.3390/catal11121429/s1: Figure S1. Parity plots and objective function values for both catalysts (a) Ir/Ni-MgO/γ-alumina and (b) $Ni_{0.5}Zr_{0.5}O_2$.

Author Contributions: Conceptualization, W.K.; methodology, W.K.; software, W.K.; validation, D.J.S. and W.L.Y.; formal analysis, W.K. and K.M.K.; data curation, K.M.K.; writing—original draft preparation, W.K. and K.M.K.; writing—review and editing, D.J.S. and W.L.Y.; funding acquisition, W.L.Y. and D.J.S. All authors have read and agreed to the published version of the manuscript.

Funding: This work was conducted under the framework of the research and development program of the Korea Institute of Energy Research (C1-2411).

Data Availability Statement: Data is contained within the article and Supplementary Material.

Conflicts of Interest: The authors declare no conflict of interest.

References

1. Lee, S.; Speight, J.G.; Loyalka, S.K. Handbook of alternative fuel technologies. In *Fuel Cells*, 2nd ed.; Chapter 16; CRC Press: Boca Raton, FL, USA, 2007; pp. 493–523.
2. Kolb, G. *Fuel Processing*; Wiley-VCH: Weinheim, Germany, 2008.
3. Ghenciu, A.F. Review of fuel processing catalysts for hydrogen production in PEM fuel cell systems. *Curr. Opin. Solid State Mater. Sci.* **2002**, *6*, 389–399. [CrossRef]
4. Jung, U.H.; Kim, W.; Koo, K.Y.; Yoon, W.L. Genuine design of compact natural gas fuel processor for 1-kWe class residential proton exchange membrane fuel cell systems. *Fuel Process. Technol.* **2014**, *121*, 32–37. [CrossRef]
5. Kim, W.; Koo, K.Y.; Lee, H.; Shul, Y.G.; Yoon, W.L. Highly dispersed nickel catalyst promoted by precious metals for CO selective methanation. *Int. J. Hydrogen Energy* **2015**, *40*, 10033–10040. [CrossRef]
6. Chen, A.; Miyao, T.; Higashiyama, K.; Yamashita, H.; Watanabe, M. High catalytic performance of ruthenium-doped mesoporous nickel-aluminum oxides for selective CO methanation. *Angew. Chem.* **2010**, *122*, 10091–10094. [CrossRef]
7. Takenaka, S.; Shimizu, T.; Otsuka, K. Complete removal of carbon monoxide in hydrogen-rich gas stream through methanation over supported metal catalysts. *Int. J. Hydrogen Energy* **2004**, *29*, 1065–1073. [CrossRef]
8. Gao, Z.; Cui, L.; Ma, H. Selective methanation of CO over Ni/Al_2O_3 catalyst: Effects of preparation method and Ru addition. *Int. J. Hydrogen Energy* **2016**, *41*, 5484–5493. [CrossRef]
9. Chen, A.; Miyao, T.; Higashiyama, K.; Watanabe, M. High catalytic performance of mesoporous zirconia supported nickel catalysts for selective CO methanation. *Catal. Sci. Technol.* **2014**, *4*, 2508–2511. [CrossRef]
10. Dagle, R.A.; Wang, Y.; Xia, G.; Strohm, J.J.; Holladay, J.; Palo, D.R. Selective CO methanation catalysts for fuel processing applications. *Appl. Catal. A* **2007**, *326*, 213–218. [CrossRef]
11. Galletti, C.; Specchia, S.; Saracco, G.; Specchia, V. CO-selective methanation over $Ru-Al_2O_3$ catalysts in H_2-rich gas for PEM FC applications. *Chem. Eng. Sci.* **2010**, *65*, 590–596. [CrossRef]
12. Liu, Q.; Dong, X.; Mo, X.; Lin, W. Selective catalytic methanation of CO in hydrogen-rich gases over Ni/ZrO_2 catalyst. *J. Nat. Gas Chem.* **2008**, *17*, 268–272. [CrossRef]
13. Zyryanova, M.M.; Snytnikov, P.V.; Gulyaev, R.V.; Amosov, Y.I.; Boronin, A.I.; Sobyanin, V.A. Performance of Ni/CeO_2 catalysts for selective CO methanation in hydrogen-rich gas. *Chem. Eng. J.* **2014**, *238*, 189–197. [CrossRef]
14. Panagiotopoulou, P.; Kondarides, D.I.; Verykios, X.E. Selective methanation of CO over supported noble metal catalysts: Effects of the nature of the metallic phase on catalytic performance. *Appl. Catal. A* **2008**, *344*, 45–54. [CrossRef]
15. Panagiotopoulou, P.; Kondarides, D.I.; Verykios, X.E. Selective methanation of CO over supported Ru catalysts. *Appl. Catal. B* **2009**, *88*, 470–478. [CrossRef]
16. Tada, S.; Kikuchi, R.; Urasaki, K.; Satokawa, S. Effect of reduction pretreatment and support materials on selective CO methanation over supported Ru catalysts. *Appl. Catal. A* **2011**, *404*, 149–154. [CrossRef]
17. Urasaki, K.; Endo, K.; Takahiro, T.; Kikuchi, R.; Kojima, T.; Satokawa, S. Effect of support materials on the selective methanation of CO over Ru catalysts. *Top. Catal.* **2010**, *53*, 707–711. [CrossRef]
18. Tada, S.; Kikuchi, R. Preparation of Ru nanoparticles on TiO_2 using selective deposition method and their application to selective CO methanation. *Catal. Sci. Technol.* **2014**, *4*, 26–29. [CrossRef]
19. Eckle, S.; Anfang, H.-G.; Behm, R.J. What drives the selectivity for CO methanation in the methanation of CO_2-rich reformate gases on supported Ru catalysts? *Appl. Catal. A* **2011**, *391*, 325–333. [CrossRef]
20. Park, E.D.; Lee, D.; Lee, H.C. Recent progress in selective CO removal in a H_2-rich stream. *Catal. Today* **2009**, *139*, 280–290. [CrossRef]
21. Mohaideen, K.K.; Kim, W.; Yoon, W.L. Highly efficient non-noble metal based nanostructured catalysts for selective CO methanation. *Catal. Commun.* **2015**, *71*, 7–12. [CrossRef]
22. Yoshida, H.; Watanabe, K.; Iwasa, N.; Fujita, S.; Arai, M. Selective methanation of CO in H_2-rich gas stream by synthetic nickel-containing smectite based catalysts. *Appl. Catal. B* **2015**, *162*, 93–97. [CrossRef]
23. Konishchev, M.V.; Potemkin, D.I.; Snytnikov, P.V.; Zyryanov, M.M.; Pakharukova, V.P.; Simonov, P.A.; Sobyanin, V.A. Selective CO methanation in H_2-rich stream over Ni-, Co- and Fe/CeO_2: Effect of metal and precursor nature. *Int. J. Hydrogen Energy* **2015**, *40*, 14058–14063. [CrossRef]

24. van Herwijnen, T.; van Doesburg, H.; de Jong, W.A. Kinetics of the methanation of CO and CO_2 on a nickel catalyst. *J. Catal.* **1973**, *28*, 391–402. [CrossRef]
25. Klose, J.; Baerns, M. Kinetics of the methanation of carbon monoxide on an alumina-supported nickel catalyst. *J. Catal.* **1984**, *85*, 105–116. [CrossRef]
26. Sehested, J.; Dahl, S.; Jacobsen, J.; Rostrup-Nielsen, J.R. Methanation of CO over nickel: Mechanism and kinetics at high H_2/CO ratios. *J. Phys. Chem. B* **2005**, *109*, 2432–2438. [CrossRef] [PubMed]
27. Loc, L.C.; Huan, N.M.; Gaidai, N.A.; Thoang, H.S.; Agafonov, Y.A.; Nekrasov, N.V.; Lapidus, A.L. Kinetics of carbon monoxide methanation on nickel catalysts. *Kinet. Catal.* **2012**, *53*, 384–394. [CrossRef]
28. Alstrup, I. On the kinetics of CO Methanation on nickel surfaces. *J. Catal.* **1995**, *151*, 216–225. [CrossRef]
29. Lim, J.Y.; McGregor, J.; Sederman, A.J.; Dennis, J.S. Kinetic studies of CO_2 methanation over a Ni/γ-Al_2O_3 catalyst using a batch reactor. *Chem. Eng. Sci.* **2016**, *141*, 28–45. [CrossRef]
30. Rönsch, S.; Köchermann, J.; Schneider, J.; Matthischke, S. Global reaction kinetics of CO and CO_2 methanation for dynamic process modeling. *Chem. Eng. Technol.* **2016**, *39*, 208–2018. [CrossRef]
31. Hubble, R.A.; Lim, J.Y.; Dennis, J.S. Kinetic studies of CO_2 methanation over a Ni/γ-Al_2O_3 catalyst. *Faraday Discuss.* **2016**, *192*, 529–544. [CrossRef]
32. Karelovic, A.; Ruiz, P. CO_2 hydrogenation at low temperature over Rh/gamma-Al_2O_3 catalysts: Effect of the metal particle size on catalytic performances and reaction mechanism. *Appl. Catal. B* **2012**, *113*, 237–249. [CrossRef]
33. Tada, S.; Kikuchi, R. Mechanistic study and catalyst development for selective carbon monoxide methanation. *Catal. Sci. Technol.* **2015**, *5*, 3061–3070. [CrossRef]
34. Miyao, T.; Shen, W.; Chen, A.; Higashiyama, K.; Watanabe, M. Mechanistic study of the effect of chlorine on selective CO methanation over Ni alumina-based catalysts. *Appl. Catal. A* **2014**, *486*, 187–192. [CrossRef]
35. Xu, J.; Froment, G.F. Methane Steam Reforming, Methanation and Water-Gas Shift: I. Intrinsic Kinetics. *AIChE J.* **1989**, *35*, 88–96. [CrossRef]
36. Twigg, M.V. *Catalyst Handbook*, 2nd ed.; CRC Press: Boca Raton, FL, USA, 1989.
37. Moe, J.M. Design of water-gas shift reactors. *Chem. Eng. Prog.* **1962**, *58*, 33–36.
38. Kim, W.; Yun, C.; Kim, Y.; Park, J.; Park, S.; Jung, K.T.; Lee, Y.H.; Kim, S.H. Modeling of a Tubular Reactor Producing Epichlorohydrin with Consideration of Reaction Kinetics and Deactivation of Titanium Silicate-1 Catalyst. *Ind. Eng. Chem. Res.* **2011**, *50*, 1187–1195. [CrossRef]
39. Ferreiro, A.I.; Rabaçal, M.; Costa, M. A combined genetic algorithm and least squares fitting procedure for the estimation of the kinetic parameters of the pyrolysis of agricultural residues. *Energ. Convers. Manag.* **2016**, *125*, 290–3300. [CrossRef]
40. The MathWorks, Inc. Optimization Toolbox™ User's Guide. 2017. Available online: https://kr.mathworks.com/help/pdf_doc/optim/optim_tb.pdf (accessed on 3 November 2021).
41. Kim, W.; Mohaideen, K.K.; Yoon, W.L. Kinetic study of CO selective methanation on nickel-based catalysts. In Proceedings of the 21st World Hydrogen Energy Conference, Zaragoza, Spain, 13–16 June 2016.